

SPECT myocardial blood flow quantitation toward clinical use: a comparative study with ^{13}N -Ammonia PET myocardial blood flow quantitation

Bailing Hsu¹ · Lien-Hsin Hu² · Bang-Hung Yang² · Lung-Ching Chen³ · Yen-Kung Chen⁴ · Chien-Hsin Ting² · Guang-Uei Hung⁵ · Wen-Sheng Huang² · Tao-Cheng Wu⁶

Received: 21 June 2016 / Accepted: 7 August 2016 / Published online: 1 September 2016
© Springer-Verlag Berlin Heidelberg 2016

Abstract

Objectives The aim of this study was to evaluate the accuracy of myocardial blood flow (MBF) quantitation of $^{99\text{m}}\text{Tc}$ -Sestamibi (MIBI) single photon emission computed tomography (SPECT) compared with ^{13}N -Ammonia (NH₃) position emission tomography (PET) on the same cohorts.

Background Recent advances of SPECT technologies have been applied to develop MBF quantitation as a promising tool to diagnose coronary artery disease (CAD) for areas where PET MBF quantitation is not available. However, whether the SPECT approach can achieve the same level of accuracy as the PET approach for clinical use still needs further investigations.

Methods Twelve healthy volunteers (HVT) and 16 clinical patients with CAD received both MIBI SPECT and NH₃

PET flow scans. Dynamic SPECT images acquired with high temporary resolution were fully corrected for physical factors and processed to quantify K1 using the standard compartmental modeling. Human MIBI tracer extraction fraction (EF) was determined by comparing MIBI K1 and NH₃ flow on the HVT group and then used to convert flow values from K1 for all subjects. MIBI and NH₃ flow values were systematically compared to validate the SPECT approach.

Results The human MIBI EF was determined as $[1.0 - 0.816 \cdot \exp(-0.267/\text{MBF})]$. Global and regional MBF and myocardial flow reserve (MFR) of MIBI SPECT and NH₃ PET were highly correlated for all subjects (global R^2 : MBF = 0.92, MFR = 0.78; regional R^2 : MBF \geq 0.88, MFR \geq 0.71). No significant differences for rest flow, stress flow, and MFR between these two approaches were observed (All $p \geq$ 0.088). Bland-Altman plots overall revealed small bias between MIBI SPECT and NH₃ PET (global: $\Delta\text{MBF} = -0.03\text{Lml/min/g}$, $\Delta\text{MFR} = 0.07$; regional: $\Delta\text{MBF} = -0.07 - 0.06$, $\Delta\text{MFR} = -0.02 - 0.22$).

Conclusions Quantitation with SPECT technologies can be accurate to measure myocardial blood flow as PET quantitation while comprehensive imaging factors of SPECT to derive the variability between these two approaches were fully addressed and corrected.

Keywords myocardial blood flow quantitation · $^{99\text{m}}\text{Tc}$ -Sestamibi dynamic SPECT · ^{13}N -Ammonia PET · coronary artery disease

Bailing Hsu and Guang-Uei Hung contributed equally to this work.

✉ Wen-Sheng Huang
wshuang01@gmail.com

✉ Tao-Cheng Wu
dcwu@vghtpe.tw

¹ Nuclear Science and Engineering Institute, University of Missouri-Columbia, Columbia, Missouri, USA

² Department of Nuclear Medicine, Taipei Veterans General Hospital, Taipei, Taiwan

³ Division of Cardiology, Shin Kong Wu-Ho Su Memorial Hospital, Taipei, Taiwan

⁴ Department of Nuclear Medicine, Shin Kong Wu-Ho Su Memorial Hospital, Taipei, Taiwan

⁵ Department of Nuclear Medicine, Chang Bing Show Chwan Memorial Hospital, Changhua, Taiwan

⁶ Cardiovascular Research Center, National Yang-Ming University, Taipei, Taiwan

Abbreviations

BMI	Body mass index
CAD	Coronary artery disease
CAG	Coronary angiography
CI	Confidence interval

DBP	Diastolic blood pressure
EF	Extraction fraction
FFR	Fraction flow reserve
HR	Heart rate
HVT	Healthy volunteers
LAD	Left anterior descending
LCX	Left circumflex
MBF	Myocardial blood flow
MFR	Myocardial flow reserve
MIBI	^{99m} Tc-Sestamibi
NH3	¹³ N-Ammonia
PET	Positron emission tomography
RCA	Right coronary artery
RMBF	Rest MBF
SBP	Systolic blood pressure
SD	Standard deviation
SMBF	Stress MBF
SPECT	Single photon emission computed tomography
VOI	Volume of interest

Introduction

Cardiac positron emission tomography (PET) with ¹³N-Ammonia (NH3) and ⁸²Rb myocardial perfusion tracers for myocardial blood flow (MBF) quantitation in absolute terms (mL/min/g) has been recognized as a powerful tool for diagnosis and prognosis of coronary artery disease (CAD) at various clinical stages [1–4]. Primarily, PET enhances detection of multi-vessel disease and subclinical abnormalities while providing prognostic information to predict patient outcomes [5–7]. In particular, non-invasive PET imaging has been considered a more precise diagnostic tool to reflect the physiological condition of myocardium than the invasive approach of fraction flow reserve (FFR) to assess coronary function [8–10]. In 2012, Gould et al. established the paradigm of flow diagram to guide the clinical interpretation of flow status connecting with pathological conditions by ⁸²Rb PET and clarified the integration of important flow data into routine clinical workflow [2]. However, despite the achievement of PET MBF quantitation, to use this tool practically remains challenging in many areas around the world (e.g. Asian countries) due to the high cost of PET myocardial perfusion tracers as the major obstacle to convince healthcare systems to embrace this technology. Recently, single photon emission computed tomography (SPECT) to perform MBF quantitation has been continuously reported and positioned as an alternative tool to evade the financial barrier of cardiac PET imaging [11–19]. Even though the image quality and interpretation confidence were traditionally higher with PET than with SPECT in many clinical situations [20, 21], the diagnostic accuracy of ^{99m}Tc SPECT is currently closer to that of NH3 or ⁸²Rb PET by several key technological advances, including novel iterative reconstruction

with full physical corrections, a semiconductor detector for enhanced photon detection, and an innovative collimator design. These advances, promising the next level of SPECT quantitation, may potentially become the mandatory component to perform SPECT MBF quantitation in the future. However, because SPECT MBF quantitation has just emerged recently, whether the quantitative accuracy by any new advanced technologies can meet the standard established by PET MBF quantitation is still being investigated [22]. Consequently, data from the direct comparison of flow values quantified by SPECT and PET modalities on the same cohorts would be necessary to address the skeptics, and strong clinical data from evidence-based studies would be the key to move the tool into practical use. In this study, we directly compared MBF quantitation with ^{99m}Tc-Sestamibi (MIBI) SPECT and that of NH3 PET on the same healthy and clinical cohorts to assess the level of accuracy of the SPECT approach. We further discuss representative clinical cases from the routine use of this clinical tool.

Methods

Patient population

This study enrolled 12 healthy volunteers (HVT) and 16 clinical patients who received both SPECT and PET flow scans within 2 weeks. The HVT group, with mean age of 37 (30 to 41) years and mean body mass index (BMI) of 24.8 (16 to 32), had no evidence of CAD as assessed by risks, history, and physical/electrocardiography examination. The clinical group, with mean age of 51 (34 to 74) years and mean BMI of 25.9 (22 to 35), presented either CAD risk factors, clinical symptoms, or both with suspected or known CAD. They were stable at the time they underwent SPECT and PET flow studies.

Table 1 Characteristics of Study Subjects

Characteristics	HVT (n = 12)	Clinical (n = 16)
Age (years)	37 (30 to 41)	51 (34 to 74)
Male	8 (67 %)	13 (81 %)
Body mass index	24.8 (16 to 32)	25.9 (22 to 35)
Hypertension	0	11 (69 %)
Hyperlipidemia	0	6 (38 %)
Diabetes	0	2 (13 %)
Tobacco use	0	2 (13 %)
Family history of CAD	0	4 (25 %)
Dyspnea	0	2 (13 %)
Angina	0	9 (56 %)
Prior PCI	0	2 (13 %)
Prior MI	0	1 (6 %)

HVT healthy volunteers, CAD coronary artery disease, PCI percutaneous coronary intervention, MI myocardial infarction

Characteristics of study subjects are listed in Table 1. This study was designed to use the HVT group to obtain the human MIBI tracer extraction fraction (EF) curve by comparing MIBI K1 and NH₃ flow. The corrective curve was applied to convert MIBI K1 to flow values for the study subjects to validate SPECT MBF quantitation. Each enrolled subject agreed to sign a written consent approved by the institutional research ethics board in Taipei Veterans General Hospital, Taipei, Taiwan.

NH₃ PET/CT MBF quantification

All PET studies were performed on a whole-body 64-slice PET/computed tomography (PET/CT) scanner (Discovery STE, GE Healthcare, USA) with 2-dimensional listmode data acquisition. Healthy and clinical subjects were imaged post an overnight fasting and refrained from caffeine-containing beverages or theophylline-containing medications for 18 h before the study. PET image data were acquired at rest and post dipyridamole vasodilator stress with peripheral intravenous bolus (5 mL in 5–10 s) administration of NH₃ doses (rest = 15 mCi, stress = 25 mCi). The rest PET scan was started 10 s prior to the rest NH₃ injection. After 1 h, the pharmacological stress PET scan was started at the 7th min post 4-min dipyridamole infusion (0.56 mg/kg) and 10 s before the stress NH₃ injection. Two CT-based transmission scans (120 kVp, 40 mA, 8 s) were respectively obtained prior to the 15-min rest PET scan and post the 15-min stress PET scan, for the purpose of attenuation correction. All dynamic PET dynamic sinograms (31 frames) were rebinned from the listmode data as 15x10 s + 10x15 s + 5x60 s + 1x380s and reconstructed with the iterative reconstruction integrating full corrections for attenuation, scatter, randoms, dead-time, geometry efficiency, and noise filtering by the manufacturer recommended protocol. For individual study, the registration of CT attenuation map with PET images was verified visually and corrected for misregistration by manual 3D translation prior to finalizing the reconstruction of dynamic PET images.

Reconstructed dynamic images of each NH₃ PET flow study were then processed with a commercially available program (Syngo MBF, Siemens, USA) dedicated to NH₃ PET MBF quantitation. The program used a two-compartment model with four kinetic parameters, including one vascular volume for spillover estimation and three transport coefficients (K1: uptake rate, K2: washout rate, and K3: metabolic rate) to calculate flow values previously developed by Hutchins et al. [23]. Each study was processed automatically with a quality control step to confirm or modify the results of automatic reorientation [24, 25]. In the program, the arterial input function was initially determined by a 10x10x10 mm volume of interest (VOI) placed on the mitral valve plane between the left ventricle and atrium post the automated process of myocardial contour. In the situation of overextension in septal wall, the program allows manual adjustment to

achieve reasonable boundary that also reforms the realistic mitral valve plane. The program presented global quantitative flow values MBF in mL/g/min for stress and rest, and MFR as stress MBF (SMBF) divided by rest MBF (RMBF). Regional values for flow and MFR were listed for the three main coronary artery territories (LAD: left anterior descending; LCX: left circumflex; RCA: right coronary artery) in the standard polar map format.

MIBI SPECT MBF quantification

SPECT flow data were acquired on a conventional dual-head SPECT scanner (ECAM, Siemens, USA) using CT images from the PET flow study for attenuation correction. The scanner equipped with 0.95 cm thickness of NaI(Tl) crystal and low-energy all-purpose collimators for gamma photon detection functioned to perform fast back-and-forth or continuous gantry rotation with a maximum speed of 10 s per rotation. A dynamic SPECT scan consisted of 10x10 s + 5x20 s + 4x60 s + 1x280 s for a duration of 12 min, and a total of 20 back-and-forth rotations were acquired to produce 1280 projection views by using acquisition parameters of continuous mode, circular orbit, low-energy all-purpose collimator, 64 × 64 matrix, 1.78 zoom factor, 5.39 mm pixel size, and multiple energy windows (126–154 keV and 109–125 keV). All subjects were scanned with the same fasting and caffeine refrained protocol as that of PET study. They received rest and dipyridamole-stress dynamic SPECT scans with two separate 5.0 mL bolus injections (5–10 s) of ^{99m}Tc-Sestamibi (MIBI) tracers as 10 mCi dose for the rest scan and 30 mCi for the stress scan. The rest SPECT scan was started 10 s prior to the rest MIBI injection, while the pharmacological stress SPECT scan was started at 7 min post 4-min dipyridamole infusion (0.56 mg/kg) and 10 s before the stress MIBI injection. The time interval between rest and stress dynamic SPECT scans was within 3–4 h. To reduce the interference of MIBI uptake in the liver, a strategy giving 300–500 mL water to each patient prior to individual MIBI injection was implemented to enhance the distance between myocardium and liver by extending the stomach volume to propel the liver. Dynamic SPECT projection data were corrected for Tc99m isotope decay and reconstructed with iterative algorithm to generate dynamic image data with full physical corrections, including noise reduction, scatter correction, resolution recovery, and attenuation correction, described in separated references [12, 13]. Additionally, angular inconsistency due to initial incoming MIBI activity into the SPECT field-of-view was corrected by compensating photon counts in empty angles using projection and forward-projection of those angles with photon counts. The registration of SPECT images and CT attenuation map from the PET/CT scan was verified visually and manually corrected for misregistration by 3D translation. The residual activity in myocardium due to the prior rest injection was

estimated from the first frame of stress dynamic images and used to subtract the residual myocardial uptake in the subsequent frames. Static perfusion images with stable MIBI uptake were extracted from the last frame (440–720 s) of dynamic images and processed to obtain myocardial boundary with ellipsoid geometry estimation and the manual determination of mitral plane. The arterial input function was automatically created by positioning a rectangular VOI (dimension = $10 \times 10 \times 40$ mm) within regions of the left ventricle and atrium with a 1:2 volume ratio and adjusted manually when needed. To quantify MIBI MBF, a two-compartment model with three kinetic parameters, including one vascular volume for spillover estimation and two transport coefficients, was used in curve fitting by numeric optimization with the Levenberg–Marquardt method. The two-compartment flow equation is:

$$C_{myo}(t) = FBV \cdot C_a(t) + (1-FBV) \cdot K1 \cdot e^{-K2 \cdot t} \otimes C_a(t) \quad (1)$$

where K1 (mL/min/g) and K2 (min^{-1}) characterizing the rate of tracer uptake from blood to myocardial tissue and the rate of tracer washout from the tissue, respectively. $C_{myo}(t)$ is the measured activity concentration in myocardium obtained from dynamic SPECT images, assumed to consist of the spillover activity from arterial input $C_a(t)$ and true myocardial uptake as a convoluted term of K1, K2, and $C_a(t)$. FBV (fraction of blood volume) is the fraction of spillover term from the blood-pool region into the myocardium region, and (1-FBV) is the rest of the activity fraction contributed by the true myocardial uptake. Prior to the kinetic modeling, the dynamic polar map from the early frame of myocardium before incoming MIBI activity into the left heart region was analyzed with two regions of interest placed in septal and lateral walls, respectively. The renormalizing factor was determined by activity ratio between these two regions and utilized to correct the activity in septal wall region due to the right ventricle spillover. Each MIBI SPECT flow study was processed with a program (MyoFlowQ, Taiwan) dedicated for SPECT MBF quantitation. The program incorporated image reconstruction and flow processing in a single platform to present global and regional quantitative flow information in polar maps.

For the HVT group, the non-linear regression of global/regional MIBI K1 and NH3 flow parameters was initially performed to derive the human MIBI tracer extraction fraction (EF) as a flow-dependent function using the Renkin-Crone model [$1.0 - a \cdot \exp(-b/\text{MBF})$]. The MIBI EF function was applied back to calculate SMBF, RMBF and MFR values for the HVT group in order to verify if any technical issue in flow conversion from MIBI K1 and EF. The same MIBI EF function was then used to convert flows for the clinical group to validate MBF quantitation in the clinical group.

Statistical analysis

Continuous variables were expressed as mean \pm standard deviation (mean \pm SD) and tested the difference of mean values by paired t-test statistics. Scatter plots for SPECT RMBF, SMBF, and MFR were created and correlated with those of PET with linear regression. Z-test was employed to test if significant difference between two correlation coefficients for global and regional analyses. Bland-Altman statistics were used to acquire difference and 95 % confidence interval (CI) of agreement (± 1.96 SD) for SPECT and PET flow parameters. Non-continuous variables from patient clinical characteristics were expressed in number and percentage. A p -value < 0.05 was considered statistically significant.

Results

Physiological states during SPECT and PET flow scans

In the HVT group, rest heart rate (HR) as (SPECT = 72.7 ± 11.9 beats per minute vs PET = 69.3 ± 9.5 , $p = 0.057$), rest systolic blood pressure (SBP) as (118.8 ± 14.5 mmHg vs. 123.7 ± 16.7 , $p = 0.082$), rest diastolic blood pressure (DBP) (79.3 ± 8.9 mmHg vs. 75.6 ± 9.5 , $p = 0.072$) were overall not significantly different. Peak-stress HR (89.3 ± 9.4 vs. 85.8 ± 0.4 , $p = 0.29$), SBP (114.4 ± 10.2 vs. 113.7 ± 11.8 , $p = 0.83$), and DBP (68.95 ± 7.7 vs. 69.4 ± 9.3 , $p = 0.78$) were also not significantly different. In the clinical group, similar findings were observed: rest HR: 68.0 ± 14.1 vs. 64.6 ± 11.2 , $p = 0.45$; rest SBP: 139.2 ± 22.1 vs. 144.1 ± 25.6 , $p = 0.33$; rest DBP: 83.0 ± 15.7 vs. 85.1 ± 21.3 , $p = 0.46$; peak-stress HR: 74.6 ± 11.8 vs. 72.5 ± 11.9 , $p = 0.53$; peak-stress SBP: 144.1 ± 25.6 vs. 136.7 ± 18.1 , $p = 0.28$; and peak-stress DBP: 85.1 ± 21.3 vs. 80.7 ± 13.1 , $p = 0.34$.

Assessment of MIBI tracer extraction fraction

Figure 1a shows the non-linear regression of global MIBI K1 and EF as functions of global NH3 MBF in the HVT group (24 flow points). Figure 1b shows the same analysis for regional MIBI K1 and EF as functions of regional NH3 MBF in the same HVT group (72 flow points). For each flow data point, MIBI EF was calculated by MIBI K1 divided by true MBF derived from NH3 PET. A strong correlation coefficient (R^2) of 0.92 and low mean square residuals (MSR) of 0.0043 were observed ($p < 0.0001$) for the global non-linear regression. Physiological parameters (a, b) fitted to the Renkin-Crone model were 0.811 (95 % CI: 0.779–0.845) and 0.261 (95 % CI: 0.167–0.354). In the regional non-linear regression, R^2 was slightly lower (0.82), but still had a low MSR (0.0088) to generate a = 0.821 (95 % CI: 0.794–0.848) and b = 0.272

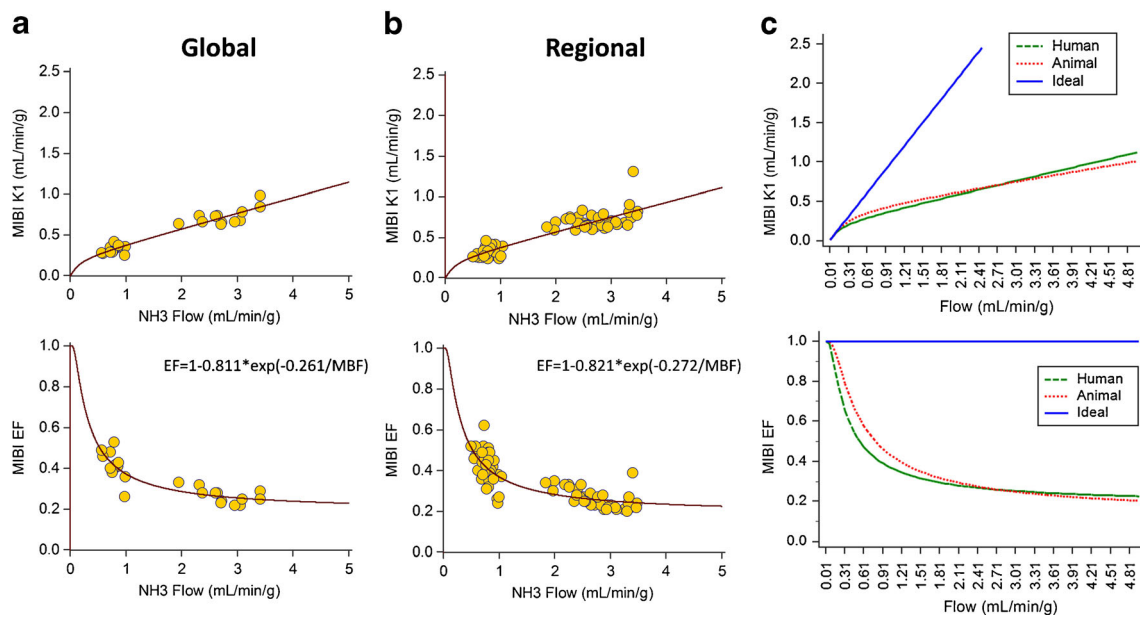


Fig. 1 Assessment of K1 and extraction fraction of MIBI tracer. **a)** global MIBI K1 and EF as a function of NH3 flow, **b)** regional MIBI K1 and EF as a function of NH3 flow, **c)** global-regional combined MIBI K1 and EF

from this study (human) compared with animal data (animal) [28, 29] and ideal characteristic (ideal). NH_3 ^{13}N -Ammonia, MIBI ^{99m}Tc -Sestamibi, K1 uptake rate (unit: ml/min/g), EF extraction fraction

(95 % CI: 0.198–0.346) ($p < 0.0001$). Both global and regional analyses demonstrated that the MIBI EF rapidly decreased with augmentation of MBF that would demand a flow-dependent correction to compensate for underestimation of flow measurement. In this study, mean physiological parameters ($a = 0.816$ and $b = 0.267$) derived from global and regional analyses determined the human MIBI EF as $[1 - 0.816 * \exp(-0.267/MBF)]$, and it was used in the subsequent flow conversion from MIBI K1 to MBF for all subjects. In comparison of human MIBI EF with the previously published MIBI EF from animal data [26, 27], the human curve presented significantly lower EF in the range of typical rest flow (~ 1.0 mL/min/g) and slightly higher EF in the range of hyperemic flow Fig. 1c. The crossing point between these two curves was 2.71 mL/min/g.

SPECT MBF Quantitation in HVT and clinical cohorts

Table 2 shows kinetic values from the curve fitting of Eq 1. for HVT and clinical cohorts. There were significant differences between rest and stress values for K1, K2, and R^2 , respectively, in the HVT group (p values: < 0.0001 , 0.011, 0.020) and the clinical group (< 0.0001 , 0.034, 0.005) as consistently higher K1, K2, and R^2 of stress than those of rest were observed. However, in comparison between HVT and clinical groups, only stress K1 encompassed significant difference ($p = 0.0082$) while there was no significant difference for all other values (all $p > 0.337$).

In the HVT group, using the human MIBI EF to convert global RMBF and SMBF, R^2 , linear slope and interception of SPECT MBF correlated with PET MBF were 0.92, 1.101, and -0.005 , as shown in Fig. 2a. Bland-Altman plot revealed small positive bias as $\Delta = 0.01$ mL/min/g (95 % CI = $-0.61 - 0.64$) (Fig. 2b). The result indicated there was no potential technical issue in the process of flow conversion from MIBI K1 and EF. Differences for mean RMBF, SMBF, and MFR values from the global myocardium between SPECT and PET approaches were overall insignificant as shown in Table 3. In the clinical group, using the same mean MIBI EF to convert global RMBF and SMBF, R^2 , linear slope and interception of SPECT MBF correlated with PET MBF were 0.90, 0.847, and 0.262 as shown in Fig. 2c. Bland-Altman plot revealed small negative bias as $\Delta = -0.06$ mL/min/g (95 % CI = $-0.58 - 0.47$) (Fig. 2d). The result indicated that flow conversion from MIBI K1 and EF can be reliable for the clinical group. Furthermore, differences for mean RMBF, SMBF, and MFR values from the global myocardium between SPECT and PET approaches were also insignificant, as shown in Table 3. Correlation coefficients of SPECT MBF and PET MBF between HVT and clinical groups were not significantly different ($p = 0.407$). In comparison of RMBF, SMBF and MFR between HVT and clinical groups, there was no significant difference for RMBF ($p = 0.747$) while significant difference for SMBF ($p = 0.0019$) and MFR ($p = 0.0001$) were observed. Similar results were also found in PET MBF quantitation (p -value: RMBF = 0.526, SMBF = 0.0005, MFR = 0.0002).

Table 2 MIBI Kinetic Values Derived from Eq 1. for HVT and Clinical Cohorts

	HVT		Clinical	
	Rest	Stress	Rest	Stress
K1 (mL/min/g)	0.32 ± 0.05	0.73 ± 0.10*	0.32 ± 0.09	0.57 ± 0.17* ⁺
K2 (1/min)	0.060 ± 0.029	0.111 ± 0.057*	0.065 ± 0.030	0.092 ± 0.039*
FBV	0.30 ± 0.10	0.34 ± 0.08	0.29 ± 0.07	0.33 ± 0.08
R ²	0.75 ± 0.09	0.82 ± 0.05*	0.72 ± 0.07	0.81 ± 0.06*

* significant difference ($p < 0.05$) from rest values in the same group;

⁺ significant difference ($p < 0.05$) between HVT and clinical groups

SPECT and PET MBF quantitation in all subjects

In combined data of HVT and clinical groups for all subjects, R², linear slope, and offset between SPECT and PET MBF were 0.92, 1.040, -0.088, and 0.78, 0.868, 0.459 for MFR comparison (Fig. 3). MBF had a higher correlation coefficient than that of MFR ($p = 0.0113$). Bland-Altman analysis revealed small negative bias as $\Delta = -0.03$ mL/min/g (95 % CI = -0.60 - 0.54) for MBF and small positive bias as $\Delta = 0.07$ (95 % CI = -0.73 - 0.87) for MFR.

Split into three vessels, regional R² and linear slope for MBF were LAD = (0.89, 1.02), LCX = (0.88, 1.03) and RCA = (0.89, 1.03) (Fig. 4). Differences among correlation coefficients of MBF in three vessels were overall insignificant (LAD vs. LCX: $p = 0.812$; LAD vs. RCA: $p = 0.98$; LCX vs. RCA: $p = 0.812$). Bland-Altman analysis revealed no bias in LAD (95 % CI = -0.67 - 0.67), small negative bias of

$\Delta = -0.07$ mL/min/g in LCX (95 % CI = -0.74 - 0.59), and small positive bias of $\Delta = 0.06$ in RCA (95 % CI = -0.60 - 0.71). Regional R² and linear slope for MFR for all study subjects were LAD = (0.78, 0.81), LCX = (0.71, 1.05), and RCA = (0.80, -0.9). Differences among correlation coefficients of regional MFR in three vessels were also insignificant (LAD vs. LCX: $p = 0.57$; LAD vs. RCA: $p = 0.85$; LCX vs. RCA: $p = 0.45$). Bland-Altman analysis revealed no bias in LAD (95 % CI = -0.84 - 0.83), positive bias of $\Delta = 0.22$ in LCX (95 % CI = -0.85 - 1.29), and small negative bias of $\Delta = -0.02$ in RCA (95 % CI = -0.83 - 0.8). Particularly, differences among correlation coefficients of regional MBF and MFR were insignificant for LAD ($p = 0.119$) and LCX ($p = 0.181$) and significant for RCA ($p = 0.042$). Figure 5 shows two examples of the report of quantitative flow result by PET and SPECT on the same HVT subject and clinical patient with three-vessel CAD.

Fig. 2 Scatter and Bland-Altman plots of global flow quantified by MIBI SPECT and NH₃ PET. **a** and **b** for the HVT group. **c** and **d** for the clinical group. Scatter plot: *solid line* linear regression; *long dash line* 95 % prediction interval; *short dash line* 95 % confident interval (CI). Bland-Altman plot: *solid line* mean difference; *long dash line* 95 % CI. MIBI ^{99m}Tc-Sestamibi, NH₃ ¹³N-Ammonia

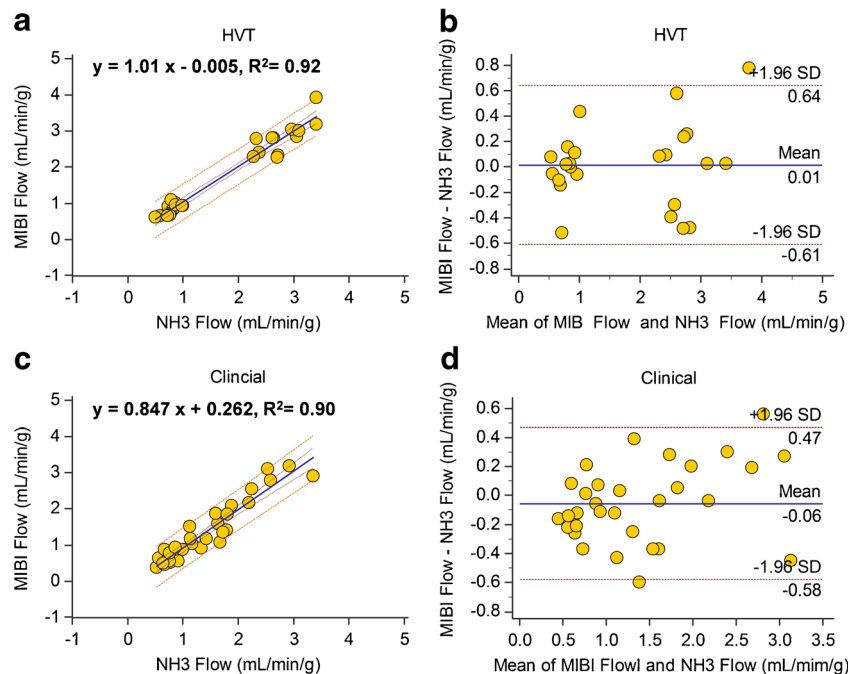


Table 3 Global Flow Values Quantified by NH3 PET and MIBI SPECT in HVT and Clinical Cohorts

	HVT			Clinical		
	NH3 PET	MIBI SPECT	<i>p</i> -value	NH3 PET	MIBI SPECT	<i>p</i> -value
RMBF (mL/min/g)	0.78 ± 0.14	0.78 ± 0.22	0.929	0.83 ± 0.24	0.74 ± 0.31	0.088
SMBF (mL/min/g)	2.80 ± 0.39	2.83 ± 0.54	0.766	1.95 ± 0.66	1.93 ± 0.78	0.813
MFR	3.58 ± 0.47	3.67 ± 0.47	0.472	2.47 ± 0.78	2.53 ± 0.72	0.601

HVT healthy volunteers, RMBF rest MBF, SMBF stress MBF, MFR myocardial flow reserve

Discussion

In this study, the kinetic modeling revealed consistently high stress K1 than rest K1 as the response to vasodilatation. Although higher stress K2 than rest K2 was also observed, MIBI washout rate represented by K2 in myocardium was on a relatively small scale compared with K1. Even though both stress and rest R² were considerably strong, higher stress R² was observed, indicating a better agreement for the pair of arterial input and myocardial time activity curves with the mathematical flow model (Eq. 1). This is expected because the stress flow data acquired from a high dose of injected MIBI (30 mCi) with higher count statistics would result in reduced random variability by lower residual image noise post noise suppression. In our study, the human MIBI EF was obtained by non-linear regression of MIBI SPECT K1 with NH3 PET flow in the HVT group (Fig. 1). The same methodology previously has been adopted to generate human EFs for Rb-82 PET tracer [30, 31]. To our knowledge, we

report the first human MIBI EF by using NH3 PET flow as the reference standard. Notably, the SPECT flow conversion for HVT subjects and compared with PET flow only served to verify if any technical issue of the method. The SPECT flow conversion for clinical cohorts was for the purpose of validation. Importantly, similar rest and stress kinetic values (K2, FBV, and R²) between HVT and clinical groups (Table 2) were first established as the requisite to use the human MIBI EF for the clinical group. To note, the flow conversion with human MIBI EF (instead of animal MIBI EF) can be substantially important to warrant the accuracy of SPECT MBF quantitation because an inappropriate EF would add a source of error (Fig. 1). Interestingly, using the human MIBI EF, RMBF from MIBI SPECT tended to be slightly lower than PET flow in the clinical group, but not in the HVT group although the difference was insignificant (*p* = 0.088). It has been reported that RMBF is highly subjective to rest hemodynamics during the dynamic flow scan [28, 29]. Likely the difference may be attributed to higher variation of rest hemodynamics between

Fig. 3 Scatter and Bland-Altman plots of global flow and MFR quantified by MIBI SPECT and NH3 in all subjects. **a)** and **b)** for flow. **c)** and **d)** for MFR. Scatter plot: *solid line* linear regression; *long dash line* 95 % prediction interval; *short dash line* 95 % confident interval (CI). Bland-Altman plot: *solid line* mean difference; *long dash line* 95 % CI. MIBI ^{99m}Tc-Sestamibi, NH3 ¹³N-Ammonia, MFR myocardial flow reserve

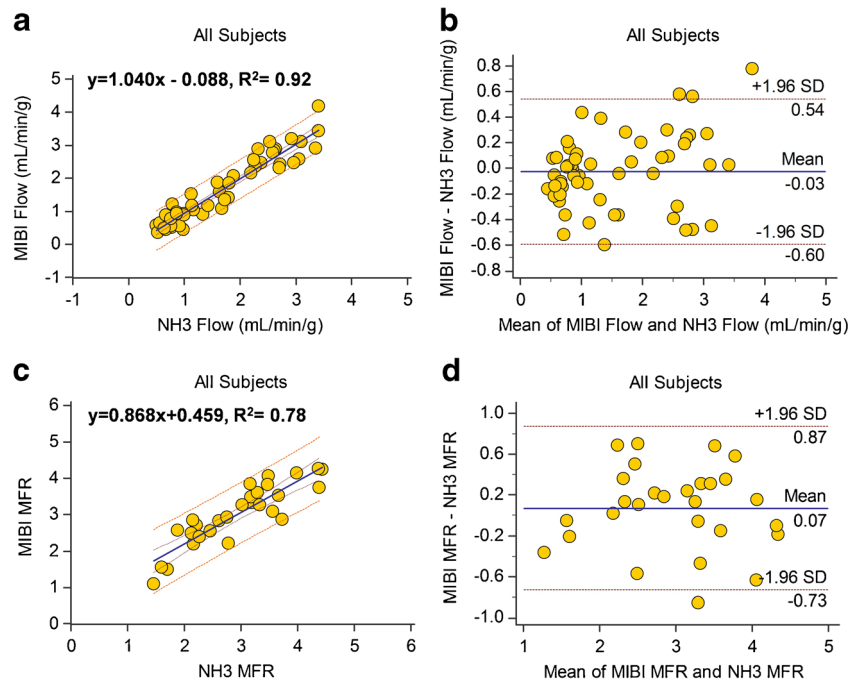
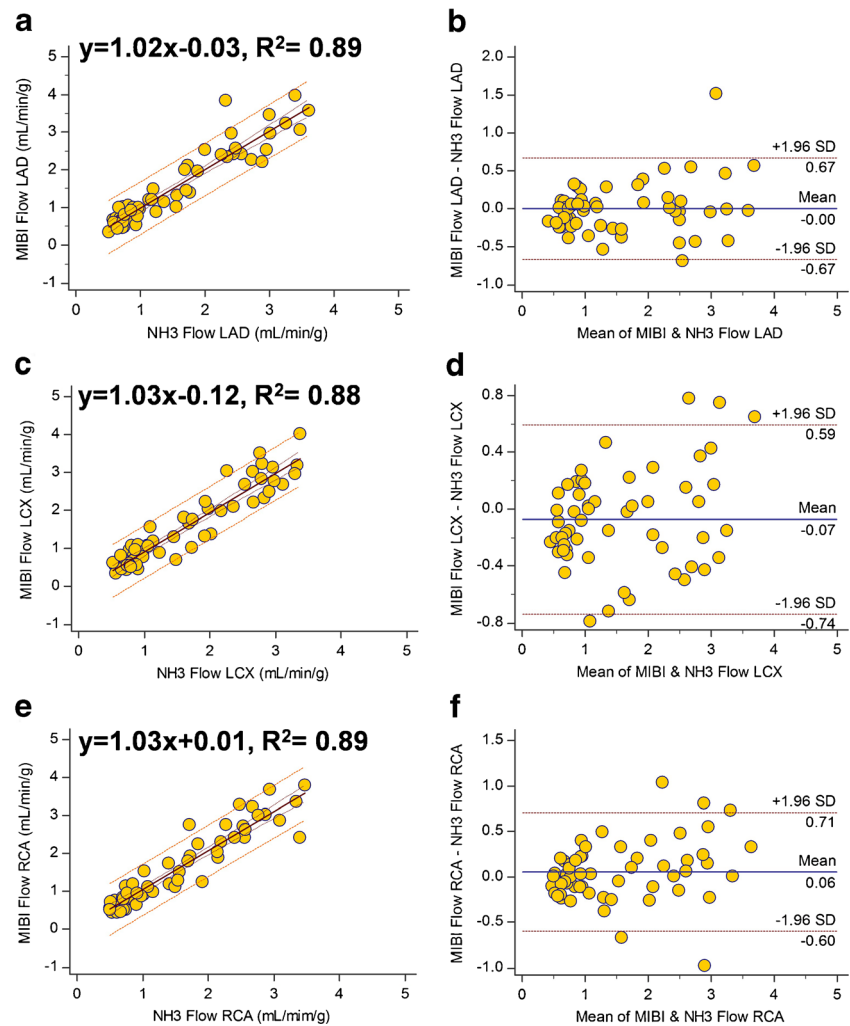


Fig. 4 Scatter and Bland-Altman plots of regional flow quantified by MIBI SPECT and NH3. **a)** and **b)** for LAD. **c)** and **d)** for LCX. **e)** and **f)** for RCA. Scatter plot: *solid line* linear regression; *long dash line* 95 % prediction interval; *short dash line* 95 % confident interval (CI). Bland-Altman plot: *solid line* mean difference; *long dash line* 95 % CI. MIBI ^{99m}Tc -Sestamibi, NH3 ^{13}N -Ammonia, LAD left anterior descending, LCX left circumflex, RCA right coronary artery



SPECT and PET scans in the clinical group ($\text{HR} \times \text{SBP}$: $\text{SPECT} = 9466 \pm 312$, $\text{PET} = 9309 \pm 287$) than in the HVT group ($\text{SPECT} = 8637 \pm 173$; $\text{PET}: 8571 \pm 159$).

Over the last few years, the motivation to develop SPECT MBF quantitation with dynamic imaging and compartmental modeling toward clinical use has been continuously demonstrated by several studies [11–17]. This intension would again address the clinical need of MBF quantitation to enhance the diagnostic accuracy of current nuclear SPECT scan. Among absolutely quantitative or semi-quantitative approaches, these studies have depicted the capability of using SPECT MBF quantitation to detect non-CAD and CAD groups [13, 17], evaluate suspected and known CAD [12, 16], or assess regional impaired flow in multi-vessel CAD patients [15]. While choosing the comparative reference to verify the performance of SPECT MBF quantitation, one study showed flow related parameter (e.g. myocardial flow reserve index) quantified by a cadmium-zinc-telluride (CZT) scanner without attenuation correction can match well with the conventional perfusion [11]. One study showed the necessity of incorporating attenuation correction, scatter correction,

resolution recovery, and noise suppression in image reconstruction for conventional dual-head SPECT scanners when invasive coronary angiography (CAG) was chosen to be the reference standard [13]. Another study showed the necessity to compensate for the image variability from attenuation, as well as other physical factors for the multi-pinhole CZT SPECT camera while FFR was chosen to validate the diagnostic performance [15]. These studies advocated the importance of applying physical corrections to reduce the imaging variability in SPECT MBF quantitation in order to move this new tool closer to a non-invasive diagnostic utility. While choosing PET MBF quantitation as the reference standard, one study demonstrated to only achieve moderate correlation ($R^2 = 0.50$) between ^{99m}Tc -Tetrofosmin (TETRO) SPECT MBF and NH3 PET MBF [14]. Notably, this study was limited by three technical issues, which may explain the dissimilar result to our study findings: 1) The study designed to derive TETRO EF from clinical patients who received SPECT and PET scans within 12 months (mean 3.3 months). After such a long period of gap, whether clinical subjects altered relevant CAD scenario between two scans was unable to justify. In our

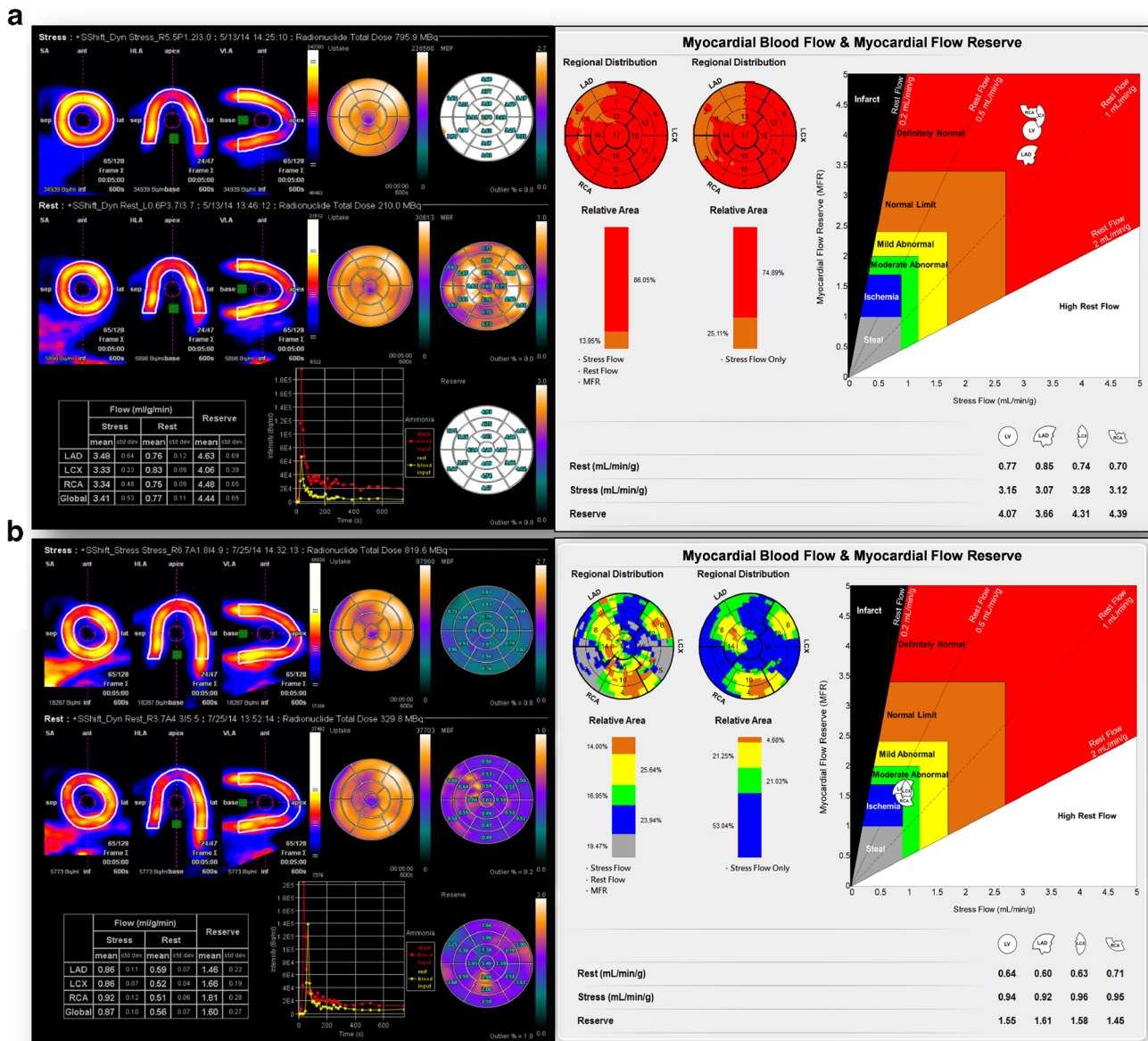


Fig. 5 Examples of quantitative flow result reported by PET and SPECT programs. **a)** HVT subject and **b)** clinical patient with three-vessel CAD by PET program (left panel: Syngo MBF) and SPECT program (right

panel: MyoFlowQ). HVT healthy volunteers, CAD coronary artery disease, LV left ventricle (global), LAD left anterior descending, LCX left circumflex, RCA right coronary artery

study, we recruited healthy volunteers presenting stable physiological stages to receive both SPECT and PET scans within 2 weeks in order to omit this variability. 2) Because of the limitation of scanner design, the dynamic SPECT acquisition (2 min per rotation) was relatively slow compared with the fast movement of tracer circulation post intravenous injection. Indeed, slow rotation of dynamic SPECT would increase angular inconsistency in early dynamic frames to potentially underestimate the arterial input. In our study, the early dynamic SPECT was as fast as 10 s per rotation to acquire dynamic data, and the correction to compensate for angular inconsistency in the early dynamic frame was implemented to further

minimize the impact. 3) Possibly also due to the limitation of scanner design, scatter correction was not performed, which can increase the magnitude of spillover between arterial blood and myocardium that may impact on the correctness of kinetic modeling. In our study, scatter correction was implemented by subtracting the scatter component estimated from a separated energy window. Overall it can be recognized that when technical variations driving the variability of SPECT and PET were addressed, the accuracy of SPECT MBF quantitation further moved close to that of PET MBF quantitation. Our study, therefore, verified that similar dynamic sampling and full physical corrections to produce quantitative image format

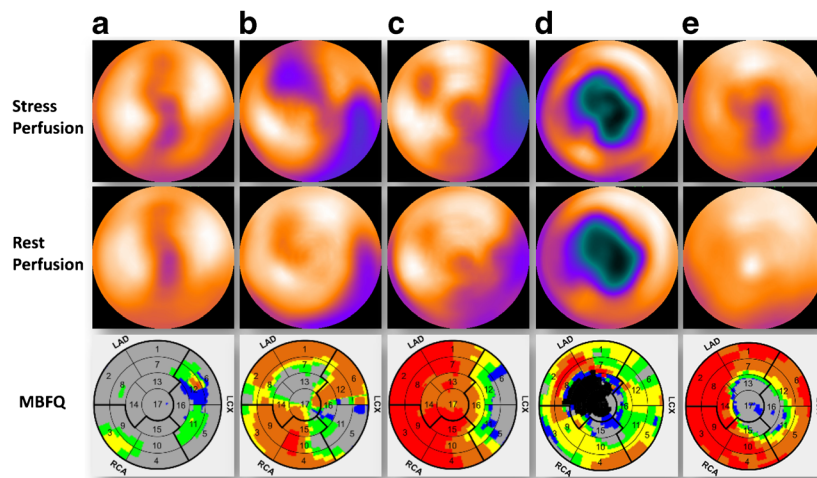


Fig. 6 SPECT perfusion and flow polar maps of representative clinical patients. **a)** three-vessel CAD, **b)** two-vessel CAD, **c)** single-vessel CAD, **d)** apical MI, **e)** apical hypertrophy. As indicated in Fig. 5, *red* represents absolutely normal flow. *Orange* represents the flow status within normal limit. *Yellow* represents the flow status within mild abnormal range.

Green represents the flow status within moderate abnormal range. *Blue* represents the flow status within the ischemic range. *Gray* represents the flow status within the flow steal range. *Black* represents MI. CAD coronary artery disease, MI myocardial infarction

would be vitally important to eliminate the imaging variability between SPECT and PET.

In our study, we carefully designed the study to optimally ensure physiological states during SPECT and PET flow scans were similar, dynamic SPECT data were acquired with the similar temporary sampling as dynamic PET, and images were reconstructed with full physical corrections prior to the kinetic modeling for flow calculation. Because of the characteristic of rapidly decreased EF at high flow range for MIBI tracer (Fig. 1), the conversion of absolute flow values from low EF would certainly introduce some degree of variability and bias. Importantly this inherent issue should be further evaluated for whether variability and bias were within the clinically acceptable norm when all relevant technical factors were addressed well. After the flow conversion, the linear regression of SPECT MBF with PET MBF for the clinical group showed a slightly underestimated slope (0.847) from unity and an offset of 0.262 mL/min/g with still a strong correlation ($R^2 = 0.90$). Nonetheless, only small bias (-0.06 mL/min/g) was observed in the Bland-Altman plot. Our study, therefore, confirmed that flow conversion with the human MIBI EF for K1 obtained from fully corrected dynamic SPECT images would be able to minimize the variability and bias in SPECT MBF quantitation within acceptable ranges.

As SPECT is demonstrated to closely measure MBF as that of PET, the next important question would be how to interpret the flow data appropriately for practical use. The MyoFlowQ program incorporates Gould's flow diagram to translate flow values into physiological conditions in variety of colors linked with disease stages [2].

Given the diagram, the interpretation of SPECT flow data is no longer complicated. Based upon our experience, we found flow findings may often override the diagnosis of perfusion studies under the circumstance of multi-vessel CAD or the perfusion study with artifacts [32]. In some clinical situations, flow and perfusion may actually provide overlapped diagnostic information. Figure 6 illustrates a list of clinical patients who received both SPECT perfusion and flow scans with clinical parameters and the related findings from CAG, echocardiography, and cardiac function, as shown in Table 4. Among them, Fig. 6a demonstrates a male patient with CAG-confirmed three-vessel CAD with unmatched flow and perfusion often observed by flow studies [4, 13, 32]. Figure 6b shows a female patient with CAG-confirmed two-vessel CAD with matched perfusion defect extent, but unmatched severity compared with the flow finding. Figure 6c depicts a male patient with CAG-confirmed severe in-stent restenosis in the LAD territory with matched extent and severity of perfusion and flow. In this particular cohort, perfusion and flow delivered the overlapped diagnostic information. Figure 6d shows a particular patient whose flow provided additional insight to detect ischemic myocardium post myocardial infarction. Figure 6e shows a male patient with echocardiography confirmed fibrotic hypertrophy and ischemia due to CAD. In this particular patient, the flow study provided additional information to assess the microcirculation in fibrotic tissue of myocardium mixed with CAD.

Because myocardial PET tracers are unavailable or economically unaffordable in Asian and many other countries, SPECT MBF quantitation has been positioned as the alternative solution to enhance the accuracy of CAD diagnosis. Our

Table 4 Patient Characteristics Corresponding to Fig. 6

Diagnosis	Age (years)	Gender	History	Risk factors	Symptoms	Angiographic Findings	Cardiac Function
A Three-vessel CAD	68	M	None	HT, HL, SM	Unstable angina, dyspnea	LAD: middle 75 %, distal 70 % LCX: proximal 90 %, middle 90 %, distal 50 % RCA: total occlusion	Stress LVEF: 57 Rest LVEF: 58
B Two-vessel CAD	66	F	PCI: LCX	HT, HL	Stable angina	LAD: distal total occlusion LCX: proximal 80 % RCA: patent	Stress LVEF: 27 Rest LVEF: 35
C Single-vessel CAD	58	M	PCI: LCX, RCA	HT, HL	Unstable angina	LAD: diffuse atherosclerosis without significant focal stenosis LCX: middle 90 % in-stent RCA: PDA 50 % in-stent	Stress LVEF: 52 Rest LVEF: 51
D Apical Infarction	69	M	MI; PCI: LAD	HT, HL, FH	Stable angina, Dyspnea	LAD: distal 80 % LCX: distal 50 % RCA: PLA 80 %	Stress LVEF: 19 Rest LVEF: 28
E Apical Hypertrophy	59	M	Medical control, Echo confirmed apical hypertrophic cardiomyopathy	HT, HL	Stable angina	LAD: patent LCX: distal 80 % RCA: patent	Stress LVEF: 59 Rest LVEF: 62

CAD coronary artery disease, M male, F female, MI myocardial infarction, PCI percutaneous coronary intervention, HT hypertension, HL hyperlipidemia, DM diabetic mellitus, SM smoking, FH family history, LAD left anterior descending, LCX left circumflex, RCA right coronary artery, PLA posterior left artery, PDA posterior descending artery, LVEF left ventricular ejection fraction, % indicates stenosis

study demonstrated that there were no internal technical limitations to prevent SPECT from delivering accurate MBF measurement like PET as previously commented [19]. Despite this encouragement, a larger scale of feasibility from evidence-based studies will still be needed to move this tool to the next level for practical use and demonstrate it as a powerful tool with a full diagnostic capacity like PET. The research protocol of SPECT MBF quantitation in the current study can be easily implemented to adopt dynamic SPECT data from current SPECT or SPECT/CT scanners capable of fast dynamic acquisition (e.g. Siemens SPECT and SPECT/CT family) or listmode data acquisition (e.g. GE 530c SPECT and 570c SPECT/CT). Technically, we think the next steps for clinical implementation would require converting the research protocol to fit into the existing routine protocol and installation of the software system to process flow data in clinical environments efficiently to meet the acceptable norm. The broad roll-out to several centers for further testing of the practical feasibility would still be needed. We strongly believe the continuous, emerging need for SPECT MBF quantitation worldwide will soon lead it to define the best clinical role in the CAD diagnosis paradigm, as well as other important applications once it is used on a routine basis.

Conclusions

Quantitation with SPECT technologies can be accurate to measure myocardial blood flow as PET quantitation, while comprehensive imaging factors of SPECT to derive the variability between these two approaches were fully addressed and corrected.

Study limitations

In this study, although we demonstrated the capability of SPECT MBF quantitation to be close to that of PET MBF quantitation, the number of investigational subjects was still small. Future study should enroll a larger number of study subjects to power the finding from this study. In addition, because our subjects were Chinese, our study didn't test SPECT MBF quantitation on patients with large BMI (>32). Whether the method of SPECT MBF quantitation in our study can be also reliable for high BMI patients still needs further investigation. The method of SPECT MBF quantitation presented in our study was only validated for SPECT scanners capable of fast dynamic acquisition and feasible for scanners capable of listmode data acquisition. Our data didn't further support the implementation for SPECT cameras without these critical capabilities.

Acknowledgments This research was supported by government research grants from Ministry of Science and Technology, Taiwan (grant numbers: NSC 102-2623-E-758-001-NU and NSC 101-2623-E-075004-NU).

Compliance with Ethical Standards

Ethical Approval All procedures performed in studies involving human participants were in accordance with the ethical standards of the institutional and/or national research committee and with the 1964 Helsinki declaration and its later amendments or comparable ethical standards.

Conflict of Interest All authors declare that they have no conflict of interest.

References

- Gould KL, Johnson NP, Bateman TM, et al. Anatomic versus physiologic assessment of coronary artery disease: guiding management decisions using positron-emission tomography as a physiologic tool. *J Am Coll Cardiol*. 2013;62:1639–53.
- Johnson NP, Gould KL. Integrating noninvasive absolute flow, coronary flow reserve, and ischemic thresholds into a comprehensive map of physiological severity. *JACC Cardiovasc Imaging*. 2012;5:430–40.
- Fiechter M, Ghadri JR, Gebhard C, et al. Diagnostic value of ^{13}N ammonia myocardial perfusion PET: added value of myocardial flow reserve. *J Nucl Med*. 2012;53:1230–4.
- Ziadi MC, Dekemp RA, Williams K, et al. Does quantification of myocardial flow reserve using rubidium-82 positron emission tomography facilitate detection of multivessel coronary artery disease? *J Nucl Cardiol*. 2012;19:670–80.
- Murthy VL, Naya M, Foster CR, et al. Improved cardiac risk assessment with noninvasive measures of coronary flow reserve. *Circulation*. 2011;124:2215–24.
- Farhad H, Dunet V, Bachelard K, et al. Added prognostic value of myocardial blood flow quantitation in rubidium-82 positron emission tomography imaging. *Eur Heart J Cardiovasc Imaging*. 2013;14:1203–10.
- Ziadi MC, Dekemp RA, Williams KA, et al. Impaired myocardial flow reserve on rubidium-82 positron emission tomography imaging predicts adverse outcomes in patients assessed for myocardial ischemia. *J Am Coll Cardiol*. 2011;58:740–8.
- Johnson NP, Kirkeeide RL, Gould KL. Is discordance of coronary flow reserve and fractional flow reserve due to methodology or clinically relevant coronary pathophysiology? *JACC Cardiovasc Imaging*. 2012;5:193–202.
- van Lavieren MA, van de Hoef TP, Sjaauw KD, et al. How should I treat a patient with refractory angina and a single stenosis with normal FFR but abnormal CFR? *EuroIntervention*. 2015;11:125–8.
- Nakazato R, Heo R, Leipsic J, et al. CFR and FFR assessment with PET and CTA: strengths and limitations. *Curr Cardiol Rep*. 2014;16:484.
- Ben-Haim S, Murthy VL, Breault C, et al. Quantification of Myocardial Perfusion Reserve Using Dynamic SPECT Imaging in Humans: A Feasibility Study. *J Nucl Med*. 2013;54:873–9.
- Klein R, Hung GU, Wu TC, et al. Feasibility and operator variability of myocardial blood flow and reserve measurements with $^{99\text{m}}\text{Tc}$ -sestamibi quantitative dynamic SPECT/CT imaging. *J Nucl Cardiol*. 2014;6:1075–88.
- Hsu B, Chen FC, Wu TC, et al. Quantitation of myocardial blood flow and myocardial flow reserve with $^{99\text{m}}\text{Tc}$ -sestamibi dynamic SPECT/CT to enhance detection of coronary artery disease. *Eur J Nucl Med Mol Imaging*. 2014;41:2294–306.
- Shrestha U, Sciammarella M, Alhassen F, et al. Measurement of absolute myocardial blood flow in humans using dynamic cardiac SPECT and ($^{99\text{m}}\text{Tc}$)-tetrofosmin: Method and validation. *J Nucl Cardiol* 2015.
- Ben Bouallègue F, Roubille F, Lattuca B, et al. SPECT Myocardial Perfusion Reserve in Patients with Multivessel Coronary Disease: Correlation with Angiographic Findings and Invasive Fractional Flow Reserve Measurements. *J Nucl Med*. 2015;56:1712–7.
- Shiraishi S, Sakamoto F, Tsuda N, et al. Prediction of left main or 3-vessel disease using myocardial perfusion reserve on dynamic thallium-201 single-photon emission computed tomography with a semiconductor gamma camera. *Circ J*. 2015;79:623–31.
- Apostolopoulos DJ, Kaspri A, Spyridonidis T, et al. Assessment of absolute $\text{Tc-}^{99\text{m}}$ tetrofosmin retention in the myocardium as an index of myocardial blood flow and coronary flow reserve by gated-SPECT/CT: a feasibility study. *Ann Nucl Med*. 2015;29:588–602.
- Petretta M, Storto G, Pellegrino T, et al. Quantitative Assessment of Myocardial Blood Flow with SPECT. *Prog Cardiovasc Dis*. 2015;57:607–14.
- Garcia EV. Are SPECT measurements of myocardial blood flow and flow reserve ready for clinical use? *Eur J Nucl Med Mol Imaging*. 2014;41:2291–3.
- Bateman TM, Heller GV, McGhie AI, et al. Diagnostic accuracy of rest/stress ECG-gated Rb-^{82} myocardial perfusion PET: comparison with ECG-gated $\text{Tc-}^{99\text{m}}$ sestamibi SPECT. *J Nucl Cardiol*. 2006;13:24–33.
- Flotats A, Bravo PE, Fukushima K, et al. ^{82}Rb PET myocardial perfusion imaging is superior to $^{99\text{m}}\text{Tc}$ -labelled agent SPECT in patients with known or suspected coronary artery disease. *Eur J Nucl Med Mol Imaging*. 2012;39:1233–9.
- Chatal JF, Rouzet F, Haddad F, et al. Story of Rubidium-82 and Advantages for Myocardial Perfusion PET Imaging. *Front Med (Lausanne)*. 2015;2:65.
- Hutchins GD, Caraher JM, Raylman RR. A region of interest strategy for minimizing resolution distortions in quantitative myocardial PET studies. *J Nucl Med*. 1992;33:1243–50.
- Pan XB, Declerck J. White Paper: Validation syngo.PET Myocardial Blood Flow. Hoffman Estates, IL: Siemens Medical Solutions; 2011:1–17.
- Pan XB, Schindler TH, Ratib O, et al. Effect of reorientation on myocardial blood flow estimation from dynamic ^{13}N PET imaging. *IEEE Nucl Sci Symp Med Imaging Conf Rec*. 2009;1:3715–7.
- Leppo JA, Meerdink DJ. Comparison of the myocardial uptake of a technetium-labeled isonitrile analogue and thallium. *Circ Res*. 1989;65:632–9.
- Klein R, Beanlands RS, deKemp RA. Quantification of myocardial blood flow and flow reserve: Technical aspects. *J Nucl Cardiol*. 2010;17:555–70. Review.
- Czernin J, Muller P, Chan S. Influence of age and hemodynamics on myocardial blood flow and flow reserve. *Circulation*. 1993;88:62–9.
- Nagamachi S, Czernin J, Kim AS, et al. Reproducibility of measurements of regional resting and hyperemic myocardial blood flow assessed with PET. *J Nucl Med*. 1996;10:1626–31.
- Lortie M, Beanlands RS, Yoshinaga K, et al. Quantification of myocardial blood flow with ^{82}Rb dynamic PET imaging. *Eur J Nucl Med Mol Imaging*. 2007;34:1765–74.
- Prior JO, Allenbach G, Valenta I, et al. Quantification of myocardial blood flow with ^{82}Rb positron emission tomography: clinical validation with ^{15}O -water. *Eur J Nucl Med Mol Imaging*. 2012;39:1037–47.
- Chen LC, Lin CY, Chen IJ, et al. SPECT Myocardial Blood Flow Quantitation Concludes Equivocal Myocardial Perfusion SPECT Studies to Increase Diagnostic Benefits. *Clin Nucl Med*. 2016;41:e60–2.